Agile beam steering using binary optics microlens arrays

William Goltsos
Michael Holz
Lincoln Laboratory
Massachusetts Institute of Technology
244 Wood Street
Lexington, Massachusetts 02173

Abstract. Agile steering of a helium-neon laser beam (λ = 632.8 nm) has been demonstrated using a complementary pair of 5-cm-aperture binary optic microlens arrays in the Galilean telescope geometry. Segmentation of a collimated input beam by illuminating approximately 60,000 $\mathcal{F}$/5 microlenses of 200-μm diameter and parabolic phase profile results in nearly aberration free beam steering over an 11° field of view for ±100-μm lateral displacements of one array relative to the other. Wavefront quality and steering efficiency of the deflected beam has been measured as a function of steering angle and is compared to a simple theoretical model.

Subject terms: active optical components; beam steering; optical scanning; diffractive optics; binary optics; microlens arrays; micro-optics.

Optical Engineering 29(11), 1392-1397 (November 1990).

CONTENTS

1. INTRODUCTION

Increasingly, micro-optic components—such as high-quality microlens arrays ($\approx 10^4$ or more lenslets of 50–400-μm diameter)—find new and attractive applications in passive and active optical sensor systems. Some applications require full imaging fidelity, and the entire microlens array must be coherent. Coherent *refractive* microlens arrays have been demonstrated with a variety of specialized fabrication techniques[1–5]; such arrays mostly offer lenslets with circular aperture having incomplete coverage (fill factors, defined as the ratio of effective lenslet to unit cell area, typically range from 20–90%). An alternative technology—binary optics—is particularly well suited for the fabrication of coherent *diffractive* microlens arrays. The array configuration need not be restricted to a simple, regular lattice; indeed, binary optics supports quite unconstrained lenslet design requirements and flexible layout. In particular, complete coverage of the entire array with functional lens area (100% fill factor) can be achieved.

Binary optics utilizes high-resolution lithography and ion-beam etching techniques to transfer binary or multistep relief patterns onto dielectric or metallic substrates. The relief structure of the lenslet functions as a highly efficient Fresnel phase zone pattern, in which circular phase gratings diffract light to a common focus. In our group, we have created computer-designed patterns for simple, aspherical, or anamorphic lenslet phase profiles and have reproduced these designs on several substrate materials with high spatial precision. Multilevel relief structures achieve high diffraction efficiency by approximating the desired continuous phase profile of the lenslet in a stepwise manner. The diffraction efficiency of a binary optics lens is fundamentally characterized by[6]

$$\eta = \left[\frac{\sin(\pi/M)}{\pi/M}\right]^2 , \qquad (1)$$

where M denotes the number of phase levels of the lens. (For example, a process with four etching steps results in a 16-level lenslet having a theoretical efficiency of 99%.) Our diffractive binary optics technology is progressing toward the utilization of 0.1-μm-accuracy lithography; this capability would permit the fabrication of high-efficiency $\mathcal{F}$/1 lenslets at *visible* wavelengths. (Recall that the smallest feature size of a Fresnel lens is given by $2\lambda\mathcal{F}/\#$.[7]) It should be remembered, however, that diffractive lens arrays, while offering design versatility and implementation ease, function as nearly ideal optical elements only over restricted bandwidths ($\approx\lambda_0 \pm 10\%$).

At present, our efforts are geared toward creating binary optic elements for specific applications. As an example, our group has demonstrated coherent laser beam addition on diode laser arrays[8] and has shown nearly ideal performance of an astigmatic lenslet array for laser diode array collimation.[9] Not restricted to microlens arrays, binary optics provides new opportunities in the design optimization and materials selection for a variety of optical elements—some performing versatile and even novel functions—such as fill factor enhancement of imaging and non-imaging detector arrays, or beam steering.

The need to randomly and rapidly steer the propagation direction of collimated laser beams, using materials with static optical properties, has motivated the design of optical systems with low rotational or translational inertia and small maximum component displacements. Agile beam steering (ABS) by microlens array (MLA) translation[10] promises to fulfill these design objectives by offering moving optical components with substrate thicknesses predicated by mechanical integrity rather than optical considerations. For a 200-μm-diameter $\mathcal{F}$/5 lenslet array set, for example, a maximum component translation of only ±100 μm achieves beam steering over an 11° field of view (FOV).

As will be shown, the unique capabilities of binary optics allow the fabrication of MLAs specifically tailored to the ABS

Invited paper AD-112 received March 24, 1990; revised manuscript received July 13, 1990; accepted for publication July 16, 1990. This paper is a revision of paper 1052-18, presented at the SPIE conference Holographic Optics: Optically and Computer Generated, Jan. 19–20, 1989, Los Angeles, Calif. The paper presented there appears (unrefereed) in SPIE Proceedings Vol. 1052.

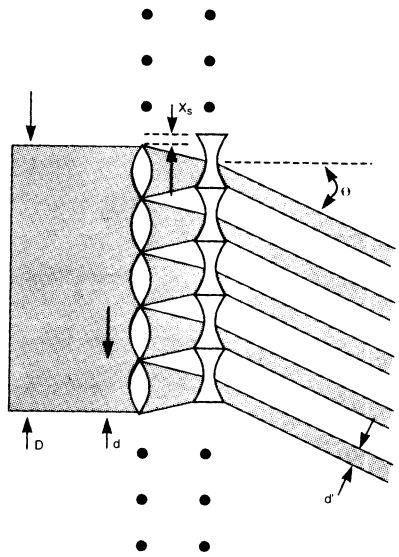

Fig. 1. Schematic illustration of light passing through an ABS MLA system. A translation of the negative MLA by x_s causes light to be deflected by the angle θ given in Eq. (2).

problem. Such MLAs impart a parabolic phase curvature on the beam segments, which substantially eliminates steering-angle-dependent wavefront aberrations in the far field.

2. MICROLENS ARRAY OPTIMIZED FOR BEAM STEERING

To illustrate the concept of beam steering by lens translation let us consider the propagation of a plane wave through a Galilean afocal lens pair. Unless both lenses are laterally centered, a plane wave incident along the system optic axis will emerge collimated but tilted to the optic axis. The tilt angle (clockwise) depends on the (upward) displacement shift x_s of the second lens with respect to the first in the plane perpendicular to the optic axis and is given by

$$\theta = -\arctan\frac{x_s}{d\,(\mathcal{F}/\#)}\,, \tag{2}$$

where d and $\mathcal{F}/\#$ are the diameter and the speed of the lens, respectively. In this scheme, large steering angles would be achieved by large lens displacements on the order of the lens diameter. In addition, significant wavefront aberrations would occur if simple spherical refractive lenses were used.

By substituting a complementary pair of MLAs with microscale lenslets in place of the macroscopic lens pair, we gain two significant advantages: First, the required translations are now greatly reduced to the order of the *lenslet* diameter—independent of the input beam diameter. Second, the lenslet phase profile can be optimized to substantially eliminate steering-angle-dependent off-axis wavefront aberrations. Such an ABS concept using a complementary pair of MLAs is schematically illustrated in Fig. 1. Let us assume that the transmittance function of the first lenslet is given by a purely parabolic phase profile, i.e.,

$$t_1(x) = \exp\left[-\frac{j\pi}{\lambda F_1}x^2\right]\,, \tag{3}$$

where F_1 is the lenslet focal length and $x = 0$ corresponds to the lenslet center; then, uniform plane wave illumination of amplitude E_0 will yield a field distribution at the plane in front of the second lenslet given by[11]

$$U_1(x) = \frac{E_0F_1}{F_2}\exp\left[-\frac{j\pi}{\lambda F_2}x^2\right]\,, \tag{4}$$

if the MLA separation is small. Here, since we require a common focus of both lenslets, the lenslet separation has been expressed in terms of the focal length of the second lenslet, F_2. Following multiplication by the conjugate transmittance function of the second lenslet,

$$t_2(x) = \exp\left[\frac{j\pi}{\lambda F_2}(x - x_s)^2\right]\,, \tag{5}$$

we find the exiting field distribution right after the second lenslet as

$$U_2(x) = \frac{E_0F_1}{F_2}\exp\left[\frac{j\pi}{\lambda F_2}x_s^2\right]\exp\left[-\frac{j2\pi}{\lambda F_2}x\,x_s\right]\,. \tag{6}$$

As before, x_s is the displacement of the second lenslet from the optic axis. The first phase term in Eq. (6) is constant and inconsequential, but the second term represents a linear phase shift across the lenslet aperture proportional to the translation x_s, i.e., a plane wave propagating at angle θ according to Eq. (2). As Eq. (6) reveals, the selection of a parabolic phase transmission profile for the lenslets results in a transmitted wavefront free of aberrations for all steering angles. Even considering the realistic model of spherical wave propagation between the first lenslet, imparting the parabolic phase retardation, and the second at a significant separation (50 μm), only small wavefront aberrations occur ($< \lambda/20$ for our specific case), and they remain independent of steering angle.

The MLA optical system sketched in Fig. 1 resembles a variable-blaze grating structure that induces a certain far-field diffraction pattern. What are the properties of this ensemble of complementary and contiguous microlenslets, respectively introducing a linear phase shift across the segmented aperture? To illustrate the nature of the far-field pattern, let us look at a simple one-dimensional analogy. From Eq. (6), the transmittance function of the MLA optical system can be written as

$$t_{\mathrm{MLA}}(x) = \mathbf{A}(x_s)\,\mathrm{rect}\left[\frac{x}{D}\right]\left(\mathrm{comb}\left[\frac{x}{d}\right]\right.$$

$$\left.\otimes\exp\left[-\frac{j2\pi}{\lambda F_2}x\,x_s\right]\mathrm{rect}\left[\frac{x}{d'(x_s)}\right]\right)\,, \tag{7}$$

where

$$d'(x_s) = \begin{cases} d\dfrac{F_2}{F_1}\,, & |x_s| < \dfrac{d}{2}\left(1 - \dfrac{F_2}{F_1}\right)\,, \\ \dfrac{d}{2}\left(1 + \dfrac{F_2}{F_1}\right) - |x_s|\,, & \dfrac{d}{2}\left(1 - \dfrac{F_2}{F_1}\right) \leq |x_s| \leq \dfrac{d}{2}\,, \end{cases}$$

and D is the diameter of the illuminated MLA aperture. The function $d'(x_s)$ describes the effective lenslet aperture size (mutual overlap area) decreasing with increasing displacement x_s.

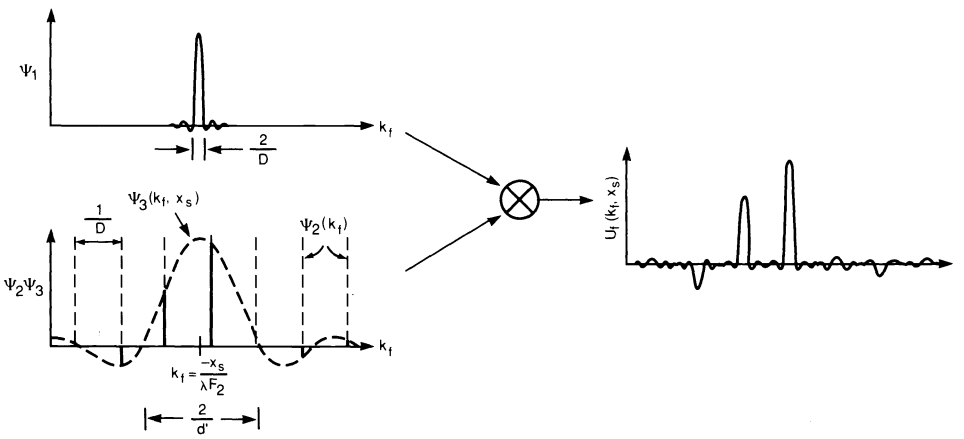

Fig. 2. One-dimensional far-field diffraction pattern of ABS MLA. Functions Ψ_i are as defined in Eq. (8). This pattern moves along the k_f axis as a function of x_s, where the sinc function width $2/[d'(x_s)]$ increases with increasing steering angle. As shown, the MLAs are not optimally aligned for maximum side-lobe attenuation.

Taking the Fourier transform yields the far-field distribution of this expression:

$$U_f(k_f,x_s) \equiv \tilde{\mathbf{A}}(x_s)\ \Psi_1(k_f) \otimes \Psi_2(k_f)\ \Psi_3(k_f,x_s) \tag{8}$$

$$= \tilde{\mathbf{A}}(x_s)\ \text{sinc}\ [k_f D] \otimes \text{comb}\ [k_f d]$$

$$\times\ \text{sinc}\left[\left(\frac{x_s}{\lambda F_2} + k_f\right) d'(x_s)\right] \tag{9}$$

$$= \tilde{\mathbf{A}}(x_s) \sum_{i=-\infty}^{\infty} \text{sinc}\left[D\left(k_f - \frac{i}{d}\right)\right]$$

$$\times\ \text{sinc}\left[\left(\frac{x_s}{\lambda F_2} + \frac{i}{d}\right) d'(x_s)\right], \tag{10}$$

where $\mathbf{A}(x_s)$ and $\tilde{\mathbf{A}}(x_s)$ are complex coefficients, $\otimes$ denotes convolution, and k_f is a normalized far-field coordinate ($k_f \equiv x_f/\lambda z$). As shown in Fig. 2, the far-field diffraction pattern consists of a linear array of discrete points, where the intensity of each point depends on the sinc function centered at $k_f = -x_s/(\lambda F_2)$ with an angular width determined by the effective array aperture D. Therefore, as the second MLA is translated by x_s, a specific point [given by Eq. (2)] of the stationary far-field grid is strongly illuminated, and a surrounding neighborhood of points is weakly illuminated according to the envelope function $\Psi_3(k_f,x_s)$. Since the effective aperture function $d'(x_s)$ of the lenslet pair decreases with increasing steering angle, the size of the weakly illuminated neighborhood increases commensurately. Also, as the one-to-one correspondence between lenslets of the first and second MLA diminishes for larger x_s, an increasingly larger fraction of light couples into a corresponding neighborhood of points at a very large deflection angle opposite the primary beam. By this consideration, the maximally useful translation shift of the MLA occurs for $x_s = \pm d/2$ at a steering angle $\theta_{\max} = \pm\arctan[1/(2\mathcal{F}/\#)]$; at this angle the primary beam and its parasitic, or conjugate, companion show precisely equal illumination.

Generalizing this result to a two-dimensional MLA system, the far-field intensity distribution consists of a grid of discrete points, where the grid symmetry reflects the MLA symmetry. As before, the angular separation between points of this grid is given by the lenslet aperture ($\propto 1/d$), and the angular width of each point depends on the illuminated MLA aperture ($\propto 1/D$). The specific number and distribution of the off-axis conjugate beams now depends on steering angle, both in azimuth and altitude, as well as the symmetry properties of the array. Figure 3 summarizes these characteristics by showing the complete set of nonparasitic far-field steering angles for a two-dimensional array of square lenslets. Since translation of the MLA can yield only variable illumination of this set of discrete steering angles, we refer to any one angle of this pattern as an addressable angle.

As a consequence of the above characteristics, MLAs intended for ABS must meet several stringent requirements. To keep the energy in neighboring points (side lobes) to a minimum, the lenslet apertures of the arrays should be maximally filled; in the ideal case, this requires an inter-MLA separation of $z = 0$ and thus $F_1 = F_2$. In practice, a nonzero separation is necessary to allow free relative translation of the MLAs. The desired maximum steering angle $\theta_{\max}$ mandates the lenslet speed, and the required steering angle quantization $\Delta\theta \approx \lambda/d$ determines the lenslet aperture. Additionally, as shown above, steering without angle-dependent aberrations can only be expected for a parabolic lenslet phase profile. These requirements are not easily realized using refractive microlens array technologies presently available, but are readily implemented using binary optics techniques.

3. MICROLENS ARRAY FABRICATION

As a demonstration of ABS using binary microlens arrays, we designed a system with 11.5° FOV and ≈4000 addressable angles on a hexagonal grid. This required a complementary MLA pair consisting of 200-μm-diameter hexagonally close-packed $\mathcal{F}$/5 microlenses. At 990-μm focal length, the second, negative lenslet array allowed a 10-μm gap between the two arrays, giving unimpeded relative translation in two dimensions. The arrays completely covered 5-cm quartz disks of 0.5-mm thickness. Figure 4 shows a picture of a few lenslets.

Fabrication of the MLAs was performed in three stages: mask fabrication, pattern transfer, and substrate etching. The first step involved designing and writing the mask patterns that corresponded to the required parabolic phase profile at the desired focal length. Three masks were required for an eight-level binary approximation of the parabolic phase profile, corresponding to a 95% efficiency expectation. Although the desired lenslet layout was on a hexagonal grid, phase patterns for only two lenslets

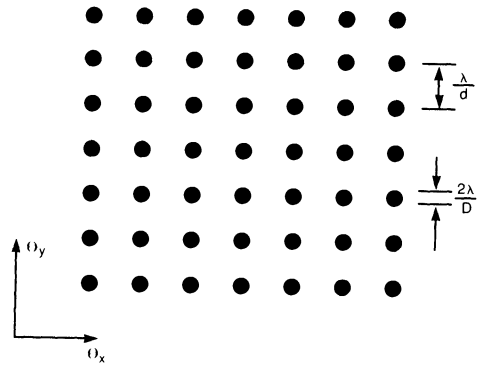

Fig. 3. Far-field steering angle pattern for a two-dimensional array of square lenslets.

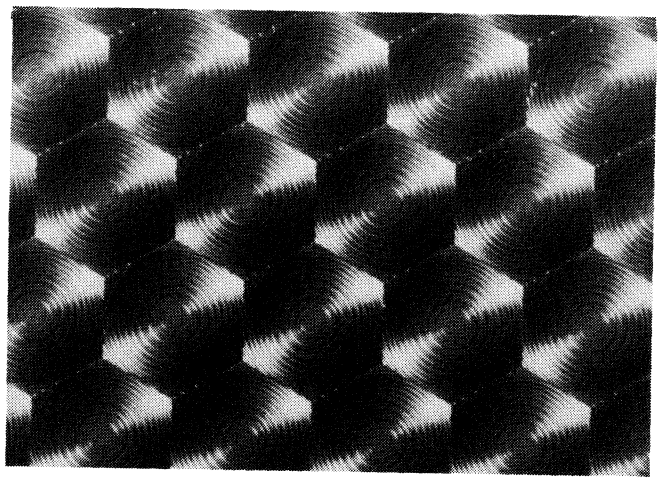

Fig. 4. Optical micrograph of lenslets in the agile beam steering array. The lenslet diameter is 200 μm, $\mathcal{F}$/5, at a density of about 3000 elements/cm².

had to be specified; the full MLA aperture was then filled by an x-y step-and-repeat process during electron-beam mask fabrication. From the masks, the patterns were copied onto the optical substrates by standard contact photolithographic techniques, followed by the final transfer into the substrate to the required depth by reactive ion etching. This expose/etch process had to be repeated three times. A more detailed description of our standard fabrication process has been published.[9]

4. PERFORMANCE OF THE BEAM STEERING MICROLENS ARRAYS

Previously, the wavefront quality of an anamorphic binary optics microlens, fabricated for efficient diode laser beam collimation, had been measured.[9] The reported rms wavefront error of better than λ/50, coupled with high diffraction efficiency, indicated high-quality optics suitable for an ABS application. However, lenslet uniformity across macroscopic scales still needed to be demonstrated for MLAs, since this property is of critical importance if diffraction-limited performance in the far field is to be attained. Therefore we measured the wavefront quality of our ABS system to test for lenslet uniformity over many lenslets. For these measurements we used a standard WYKO Ladite interferometer, which restricted the test area to a 6-mm diameter.

The test setup consisted of a spatially filtered beam from a helium-neon laser that was expanded to 3 cm and recollimated as the input beam to the beam steering MLAs. Relative position

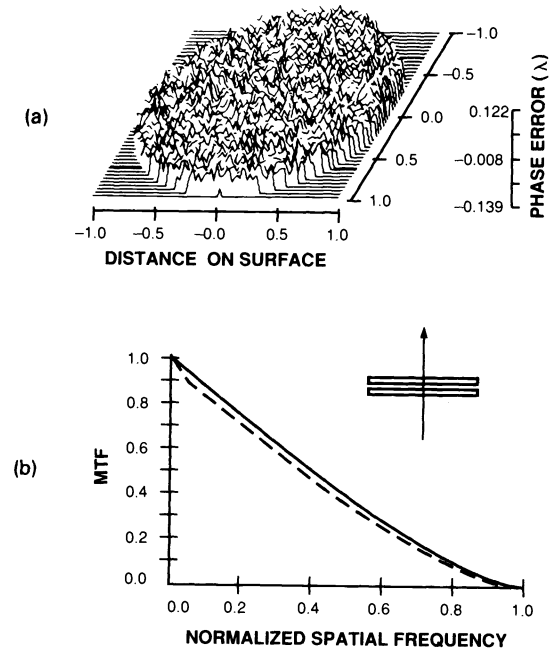

Fig. 5. Interferometer measurements of the ABS system at 0° steering angle (as depicted in the schematic). The wavefront profile and MTF are shown in (a) and (b), respectively. In (b) the solid curve shows the diffraction limit and the dashed curve is the experimental result. The measured rms phase error is λ/30 and the Strehl ratio is 0.96.

and angular orientation of the array pair could be adjusted by way of piezoelectrically driven two-dimensional translation stages and a manually positioned rotation stage. By careful alignment, we achieved minimum side-lobe energy in the far field for all steering angle configurations. We noted empirically that a rotational misalignment between the two MLAs of up to 0.5° could be tolerated for the 6-mm test aperture. The steered beam emerging from the MLA pair propagated 1 m before entering the 6–mm entrance aperture of the interferometer. Graphs of the wavefront profile and MTF for 0° steering angle are shown in Fig. 5. The measured rms error of λ/30 and Strehl ratio of 0.96 indicate essentially diffraction-limited performance and imply very high uniformity of all 900 lenslets within the 6-mm aperture. The overall measured throughput efficiency was 49% (discounting MLA reflection losses).

Using the same methods, we also measured the wavefront profile for two other beam steering configurations: at 10 addressable angles off axis (with the input beam on axis) and at 1 addressable off-axis angle. (One addressable angle corresponded in our ABS system to ≈0.18° angular quantization.) The latter case was achieved by aligning the two arrays on axis (0° steering angle) and subsequently misaligning the input beam; with this configuration we thereby simulated vernier beam steering, as might be presented by a situation in which a scanning mirror inserted before the MLA system could serve for angle interpolation between addressable angles. Figures 6 and 7 list the measured MTF and Strehl ratios for these two configurations, respectively. Again, these results confirm predominantly aberration-free beam transmittance over steering angles up to $\theta_{max}/3$. Constraints of the optical setup prevented measurements at larger deflection angles.

By "beam steering efficiency" we here mean the ratio of light power in the central target spot to the entire beam power incident on the MLA ABS system. Equation (8) shows that, for

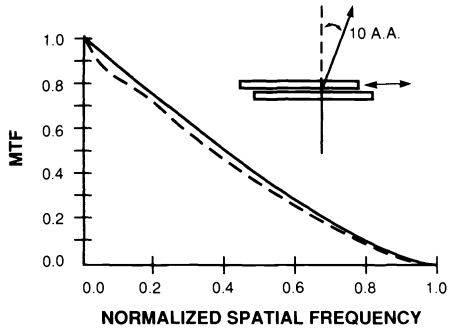

Fig. 6. Measured MTF of the ABS system at 10 addressable angles (A.A.) off-axis. One addressable angle (λ/d) ≈ 0.18°. The schematic indicates the experimental steering configuration. The rms phase error and Strehl ratio are λ/24 and 0.94, respectively.

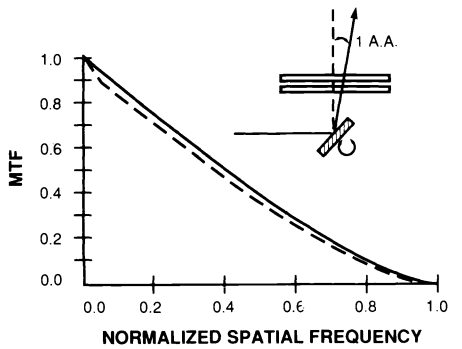

Fig. 7. Measured MTF of the ABS system when steered to 1 addressable angle (A.A.) off-axis by a scanning mirror before the arrays, as indicated in the schematic. The rms phase error measured in this configuration is λ/26 and the Strehl ratio is 0.95.

an underfilled lenslet aperture, energy is diffracted into neighboring points of the far-field pattern even for the on-axis case. To find the power in the central spot, one can determine the main-lobe coefficient of the Fourier series expansion of Eq. (7). For all steering angles, the steering efficiency is effectively

$$\eta(x_s) = \frac{f(x_s)^2}{f(x_s = 0)}, \tag{11}$$

where $f(x)$ is the x_s-dependent array fill factor. This function is equal to the area of the effective overlap of one positive lenslet with its corresponding negative lenslet, normalized by the lenslet area (see the diagram in Fig. 8). For the close-packed hexagonal lenslet geometry, the steering efficiency becomes

$$\eta_{\text{hex}}(x_s) \approx \frac{\left[(1-\delta)^2 - \frac{4x_s}{3d}(1-\delta) + \frac{1}{3}\left(\frac{x_s}{d}\right)^2\right]^2}{(1-\delta)^2} \tag{12}$$

for small δ; here δ is the fixed percentage of lenslet underfill caused by the finite array separation. For our system δ = 10/1000 = 0.01, corresponding to 1000-μm focal length and 10-μm separation.

The steering efficiency described by Eq. (12) implies 100% efficiency for each lenslet. For binary optic lenses, the attainable lenslet diffraction efficiency depends, among other factors, on the number of quantization levels in the phase profile approximation. The test MLAs had been etched to eight levels, corresponding to a 95% efficiency expectation. Due to mask misalignment and etching errors accumulated during fabrication, the actual diffraction efficiencies for the positive and negative array were measured to be 84% and 72%, respectively. Under optimum circumstances, the overall on-axis steering efficiency for this MLA pair was therefore constrained to be ≤59%, including the underfill factor of Eq. (12).

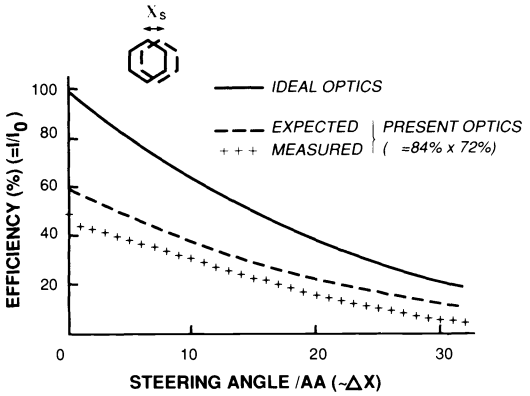

Fig. 8. ABS efficiency as a function of steering angle (normalized to 1 addressable angle). The solid and dashed curves show the theoretical efficiency according to Eq. (12) for 100% and the experimentally expected 59% diffraction efficiency of a lenslet pair, respectively. The + marks are experimentally measured values.

Figure 8 summarizes the results after scaling the experimental data for reflection losses. The ideal 100% efficient lenslet case of Eq. (12) is plotted as the solid curve (with δ = 0.01). The dashed curve (expected steering efficiency) was derived from Eq. (12) by 59% scaling. The + marks represent the efficiency measurements at each addressable angle, obtained by measuring the central spot power relative to the total incident input power.

While the measurements follow the trend of the efficiency prediction overall, the presence of an angle-dependent scale factor between expected and measured results is indicated. Since we have demonstrated good wavefront quality, largely independent of steering angle, we are inclined for the following reason to attribute the observed angle dependence of the effective efficiency to a radially dependent efficiency loss of the individual lenslets: At larger translations x_s, light diffracted into the steering angle emerges from the MLA increasingly only through the outer regions of each lenslet pair. These edge areas exhibit the finest surface features and thus are most susceptible to fabrication errors, leading to a reduced effective diffraction efficiency.

To maintain large FOV coverage with reasonable efficiency demands high-speed microlenses, as illustrated in Fig. 9, where we graph the optimal case of Eq. (12), parameterized by $\mathcal{F}/\#$. The efficiency curves in Fig. 9 terminate at the angle $\theta_{\max}$. We see that an $\mathcal{F}/1$ ABS system could achieve steering over 53° FOV ($2\theta_{\max}$) with an efficiency exceeding 50%. While the projected optical performance of high-speed MLA systems appears attractive, we caution that the practically achievable beam steering efficiency is less. As mentioned, factors such as intrinsic effects, considerations of design practicality, and fabrication-related deficiencies diminish the overall achievable efficiency of the ABS system.

Fabrication-related errors that curtail binary lens performance have been identified and measured. One set of errors occurs during mask fabrication: the patterns generated during the electron beam mask-writing process exhibit round-off and DAC linearity errors and stepper positioning inaccuracies. A second group of errors can occur during the transfer process of the mask

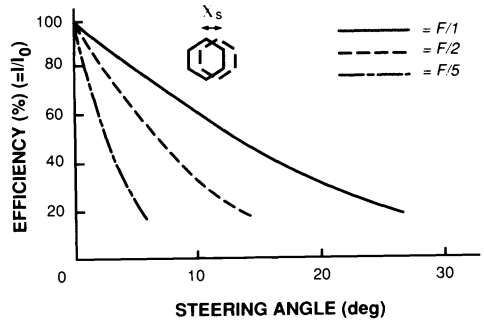

Fig. 9. Theoretical ABS efficiency as a function of steering angle for several lenslet speeds, assuming ideal optics. Curves are given by Eq. (12) together with Eq. (2) and $\delta = 0$.

patterns into the substrate: these errors involve variations in the resist exposure, development, and reactive ion etching procedures, and the mask position repeatability. Accurate alignment of successive masks for multilevel structures is of critical importance. Cumulative fabrication errors currently limit our practically attainable minimum feature size to ≈ 0.4 μm, but efforts are continuously under way to further minimize all of the above error sources.

5. CONCLUSIONS

Agile beam steering over an 11.5° FOV has been demonstrated for a 6-mm He-Ne beam, using a microlens-array-based optical system with ± 100-μm maximum travel and ≈ 35-Hz sweep rate. Mechanical resonances in the nonoptimized PZT-actuated drive system limited the angular speed to ≤ 400°/s. The measured diffraction-limited performance indicated very high lenslet uniformity across the array aperture and underscored several unique capabilities of the binary optics technology. Measured efficiency and steering performance fall in agreement with a simple model by taking certain identified error sources into account.

While such a performance level is about an order of magnitude below the capability of well-engineered, commercially available galvanometric systems,[12] we like to point to the paucity of practical concepts for *agile* beam steering, as opposed to repetitive or raster scan systems—particularly when taking the requirement of "static optical properties" into consideration.

As a brief list of alternative approaches (other than galvanometer-based systems and without regard for completeness), we can cite a phase diffraction concept based on domain switching in magneto-optic garnet films[13] and the demonstration of arrays of micrometer-sized mirrors, individually deformable by CCD addressing schemes.[14] Both of these approaches seem to involve specific design parameter restrictions that are somewhat orthogonal to the constraints of the MLA approach, and they have been publicly demonstrated in a more restricted parameter space than the present work. Being concerned with achieving a viable demonstration and an objective assessment base, we did not invest any serious efforts on system design optimization.

All three approaches share two very desirable characteristics: (1) the critical element fabrication is principally based on integrated circuit processing techniques with all their advantages (and complications); (2) the critical elements should offer practical scalability to large-scale aperture sizes.[15] They also impose specific design restrictions and trade-offs. Which of these (or other) techniques is the "right" approach is beyond the scope of our work and can be properly decided only in the context of concrete real-world applications.

6. ACKNOWLEDGMENTS

We thank William Delaney, Marsden Griswold, Philip Bundman, and Miles Scott for fabricating the diffractive microlens array pair; we and this project benefited from numerous interactions with James Leger and Gary Swanson and the generous support and guidance of Wilfrid Veldkamp. We also acknowledge Paul Temple, formerly of NWC/SCIO, for sponsoring this work.

This work was sponsored by the Strategic Defense Initiative Organization. The views expressed are those of the authors and do not reflect the official policy or position of the U.S. government.

7. REFERENCES

1. N. F. Borelli, D. L. Morse, R. H. Bellman, and W. L. Morgan, "Photolytic technique for producing microlenses in photosensitive glass," Appl. Opt. 24, 2520–2525 (1985).
2. Z. D. Popovic, R. A. Sprague, and G. A. N. Connell, "Technique for monolithic fabrication of microlens arrays," Appl. Opt. 27, 1281–1284 (1988).
3. M. Oikawa, K. Iga, S. Misawa, and Y. Kokubun, "Improved distributed-index planar microlens and its application to 2-D lightwave components," Appl. Opt. 22, 441–442 (1983).
4. I. N. Ozerov, V. M. Petrov, V. A. Shishkina, and V. M. Shor, "Shaping the contours of dies for manufacturing lens arrays having spherical elements," Sov. J. Opt. Technol. 48, 49–50 (1981).
5. Z. L. Liau, V. Diaduk, J. N. Walpole, and D. E. Hull, "Large-numerical aperture InP lenslets by mass transport," Appl. Phys. Lett. 52, 1859–1861 (1988).
6. G. J. Swanson, "Binary optics technology: The theory and design of multilevel diffractive optical elements," Lincoln Lab. Tech. Rep. 854, August 14, 1989.
7. L. d'Auria, J. P. Huignard, A. M. Roy, and E. Spitz, "Photolithographic fabrication of thin film lenses," Opt. Commun. 5, 232–235 (1972).
8. J. R. Leger, M. Holz, G. J. Swanson, and W. Veldkamp, "Coherent laser beam addition: an application of binary-optics technology," Lincoln Lab. J. 1, 225–246 (1988).
9. J. R. Leger, M. L. Scott, P. Bundman, and M. P. Griswold, "Astigmatic wavefront correction of a gain-guided laser diode array using anamorphic diffractive microlenses," in *Computer-Generated Holography II*, S. H. Lee, ed., Proc. SPIE 884, 82–89 (1988).
10. J. K. Bowker, "A general theory of dual gratings (a one-dimensional analysis for agile beam errors)," Technical Memo, August 4, 1987.
11. See, for example, J. W. Goodman, *Introduction to Fourier Optics*, p. 88, McGraw-Hill, New York (1968).
12. See, for example, G. F. Marshall, *Laser Beam Scanning*, p. 222, Table 9, Marcel Dekker, New York (1985).
13. G. L. Nelson et al., "Stripe domain light deflection for intersatellite communications," in *Communications Networking in Dense Electromagnetics Environments*, K. Wu, ed., Proc. SPIE 876, 121–129 (1988).
14. R. W. Cohn and J. B. Sampsell, "Deformable mirror device uses in frequency excision and optical switching," Appl. Opt. 27, 937–940 (1988).
15. An impressive demonstration of ABS on a 2-m mirror is described by S. E. Forman and R. A. LeClair, "Lightweight mirror structures for mechanical beam steering," Lincoln Lab. J. 1, 133–144 (1988).

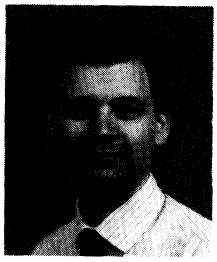

William C. Goltsos is a staff member in the Laser Radar Measurements Group at MIT/Lincoln Laboratory. His interests include developing binary optics fabrication techniques and applying diffractive optics to solid-state laser systems. He received a BS degree in physics from Rensselaer Polytechnic Institute, and MS and Ph.D. degrees in physics from Brown University.

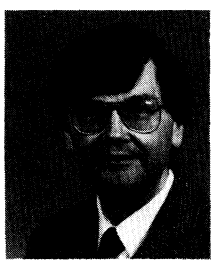

Michael Holz is a staff member in the Laser Radar Measurements Group. His work spans the areas of binary optics, laser beam addition, laser physics, and neural networks. Before joining Lincoln Laboratory, he worked on a ring laser gyroscope at Raytheon Research. He received a Physics Diploma from the Technical University of Munich and a Ph.D. in physics from MIT. He encourages children to develop an appreciation of science and performs science demonstrations at schools.